2018 European Control Conference (ECC)
June 12-15, 2018. Limassol, Cyprus

Optimal Setpoint Computation for Constrained Torque Control of PMSMs

Tobias Englert, and Knut Graichen

Abstract— **Many torque control schemes for permanent magnet synchronous machines require suitable reference values for the dq-currents. This contribution presents an algorithm to compute these references in an optimal and computationally efficient manner. The algorithm relies on the steady state dq-model with stator resistance and accounts for nonlinear constraints on the phase currents and voltages as well as on the DC link current, which is of relevance e.g. for battery management systems. The algorithm requires a minimum computation time to ensure real-time feasibility for PMSM torque controllers. Simulation results and computation times of less than 10 µs on CPU and dSpace level illustrate the performance of the algorithm and its suitability for an embedded real-time implementation.**

I. INTRODUCTION

Permanent magnet synchronous machines (PMSMs) are becoming increasingly popular in various application domains due to their excellent power density and efficiency. These characteristics make PMSMs particularly suitable for high power and performance applications such as wind turbines, machine tools, or electric power steering systems.

A typical control task for PMSMs is torque control. Various control strategy are proposed in the literature in order to track a desired torque. Besides classical field orientated control, cf. e.g. [1], Lyapunov-based controller [2], flatness-based controller [3] as well as model predictive control (MPC) schemes [4], [5], [6], [7], [8] have been developed.

The majority of PMSM control strategies require a reference current computation. On the one hand, many torque controls actually rely on a current control, cf. e.g. [9], which depend on reference values to track the desired torque and to ensure compliance with the system constraints, at least approximately. On the other hand, some of the MPC approaches, e.g. [8], utilize the reference values to improve the controller's robustness and stability.

A couple of strategies for computing reference currents have been developed in the past. In [10] and [11], energy efficient reference values for a desired torque are computed offline and stored in look-up tables. However, these maps grow in size and complexity if field weakening effects or variable DC link voltages shall be taken into account. Further approaches propose to vary the field weakening angle depending on the dq-voltages or to introduce an additional voltage control. Potential issues in this regard are the overall stability of the control scheme, slow transient responses and a non-energy-optimal operation. For a more detailed discussion see e.g. [12].

The authors are with the Institute of Measurement, Control and Microtechnology, Ulm University, Germany.
E-mail: <firstname>.<lastname>@uni-ulm.de

In contrast to these approaches, other recent publications [12], [8] are based on the online solution of a nonlinear constrained optimization problem. However, these methods either consider only a part of the whole operating range of the PMSM or neglect the stator resistance in order to simplify the problem formulation. These simplification, however, again lead to a suboptimal operation of the motor in terms of energy efficiency, in particular in field weakening operation, where the large currents lead to large model deviations if the stator resistance is neglected. In addition, none of the aforementioned methods consider constraints on the DC link current. These constraints, however, are especially relevant in automotive applications, where the battery current is dynamically limited by a battery management system (BMS).

This paper presents an algorithm for computing reference current values for PMSMs that account for these constraints. The approach is based on a nonlinear constrained optimization problem, which can be solved analytically in a combinatorial manner. To this end, the optimization problem is divided into a number of subproblems that allows one to determine the optimal solution in a computationally efficient way. The minimal computation footprint of the algorithm in terms of CPU time and memory requirement is particularly important for PMSM torque control, as the control hardware is typically very limited in practice, while the sampling times for controlling electric drives are in the submillisecond range. In order to prove the performance of the algorithm, the paper provides simulation and runtime results on a standard PC as well as on a dSpace real-time platform. The obtained computation times of less than 10 µs indicate the real-time implementability on embedded or low-level control hardware, e.g. electric control units (ECUs) in automotive applications.

The paper is organized as follows: Section II introduces the drive system, the dq-model, and the different system constraints to be accounted for. Section III then formulates and investigates the nonlinear constrained optimization problem for the reference current values. The algorithm for the online solution of the optimization problem is derived in Section IV, before runtime time and simulation results are presented in Section V. A short summary and an outlook to further work is finally given in Section VI.

II. PMSM MODEL AND CONSTRAINTS

The computation of the PMSM reference currents for a desired torque is based on the well-known dq-model and has to account for several constraints that are shortly introduced in the following lines.

978-3-9524-2699-9 ©2018 EUCA

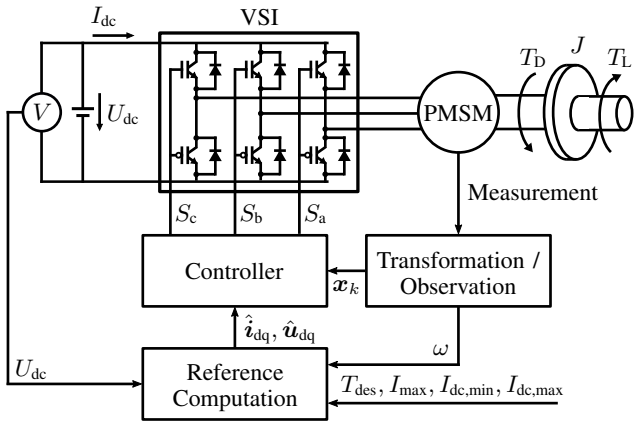

Fig. 1. Schematic representation of the PMSM drive system.

A. PMSM model

Fig. 1 gives an overview of the considered PMSM system. The motor is driven by a voltage source inverter (VSI), which is controllable via the switching signals S_a, S_b, S_c. The VSI is connected to a DC circuit with DC link voltage U_{dc} and DC link current I_{dc}. The PMSM itself is described by the well-known dq-model, see e.g. [1],

$$L_d \tfrac{d}{dt} i_d = -R_s i_d + L_q \omega i_q + u_d \tag{1a}$$

$$L_q \tfrac{d}{dt} i_q = -R_s i_q - L_d \omega i_d - \omega \psi_p + u_q \tag{1b}$$

$$J \tfrac{d}{dt} \omega = \left(T_D(i_d, i_q) - \tfrac{\mu_f}{z_p} \omega - T_L \right) z_p \tag{1c}$$

with the dq-currents i_d and i_q, the electrical rotor speed ω, the dq-voltages u_d and u_q, the load torque T_L and the driving torque

$$T_D(i_d, i_q) = \tfrac{3}{2} z_p \left(\psi_p i_q + i_d i_q (L_d - L_q) \right) \tag{2}$$

that is generated by the PMSM. The system parameters are the number of pol-pairs z_p, the stator resistance R_s, the dq-inductances L_d, L_q, the permanent flux linkage ψ_p, the total moment of inertia J, and the friction coefficient μ_f.

As indicated in Fig. 1, we assume the existence of a torque controller, see e.g. the references in Section I, that typically requires the measurement or estimation of the state vector $\boldsymbol{x}_k = [i_{d,k}, i_{q,k}, \omega_k]^T$ at the sampling instance t_k, and utilizes reference values for the dq-currents $\hat{\boldsymbol{i}}_{dq} = [\hat{i}_d, \hat{i}_q]^T$ in order to adjust a desired value T_{des} for the driving torque T_D. Depending on the actual controller design, the corresponding stationary voltages $\hat{\boldsymbol{u}}_{dq} = [\hat{u}_d, \hat{u}_q]^T$ might be of interest as well. The values $(\hat{\boldsymbol{i}}_{dq}, \hat{\boldsymbol{u}}_{dq})$ are provided by the reference computation block in Fig. 1 that requires the electrical rotor speed ω, the DC link voltage U_{dc}, the desired torque T_{des} as well as the maximum values of the constraints that are detailed in the following Section II-B. In addition, the reference computation block requires knowledge of whether the PMSM is operated in motor or generator mode. This can be internally checked in terms of absorbed or delivered mechanical power, i.e.

$$\omega \, T_{des} \geq 0 \quad \text{or} \quad \omega \, T_{des} < 0 \, . \tag{3}$$

Note that the electrical parameters in the dq-model (1) are not necessarily constant. The stator resistance R_s typically depends on the temperature, which, however, is slowly varying w.r.t. to the dq-current dynamics. Moreover, the dq-inductivities L_d and L_q as well as the permanent flux linkage ψ_p depend on the dq-currents $\boldsymbol{i}_{d,q}$ and the rotor angle φ, see e.g. [13], [14]. Considering these dependencies would lead to a far too complex model for an online reference value computation. However, the parameters may be adapted according to the current system state to improve the reference currents. Finally, parasitic effects of the VSI are neglected as well, though e.g. an additional resistor can be introduced easily in order to model VSI switching losses.

B. System Constraints

There are several constraints for an efficient PMSM control that the reference computation has to take into accounts. The three phase currents (i_a, i_b, i_c) are typically limited by $|i_l| \leq I_{max}$, $l \in \{a,b,c\}$, either by the VSI or by the motor itself. A primary operating strategy may change the limit I_{max} at runtime in order to take advantage of the component's thermal capacities, cf. [15]. A transformation of these constraints leads to the following spherical inequality in the dq-coordinate system

$$i_{abs}^2 = i_d^2 + i_q^2 < I_{max}^2 \, . \tag{4}$$

A further constraint concerns the phase voltages. As a consequence of the VSI design with three legs and two possible switching states (cf. Fig. 1), eight voltage vectors can be applied to the motor. Typically, a modulation scheme is used to access the whole (u_d, u_q)-hexagon that is spanned by the eight primary voltage vectors [1]. It is common practice to approximate the hexagon by its inner circle leading to the inequality [2]

$$u_{abs}^2 = u_d^2 + u_q^2 \leq U_{max}^2 = \tfrac{1}{3} U_{dc}^2 . \tag{5}$$

In addition to the phase currents and voltage constraints, the DC link current I_{dc} is often limited by a primary operating strategy, e.g. given by a BMS, and may additionally vary at runtime. The DC link current I_{dc} is often restricted to a non-symmetrical interval, i.e. $I_{dc,min} \leq I_{dc} \leq I_{dc,max}$, which can be expressed as

$$I_{dc,min} \leq \tfrac{3}{2} \tfrac{(i_d u_d + i_q u_q)}{U_{dc}} \leq I_{dc,max} \tag{6}$$

using a simple power balance consideration. In summary, (4)-(6) represent nonlinear constraints for both the dq-currents and the dq-voltages that have to be satisfied by references that are provided to the controller, cf. Fig. 1.

III. Optimization Problem

The reference values for the currents $\hat{\boldsymbol{i}}_{dq}$ and voltages $\hat{\boldsymbol{u}}_{dq}$ for a desired driving torque T_{des} are determined by solving a nonlinear constrained optimization problem that is outlined

[1] Note that two of the eight voltage vectors are zero vectors.

[2] Although the reference current computation uses the spherical formulation of the voltage constraint (5) that is motivated by a modulation scheme, the reference currents can also be used in case of a direct VSI actuation, e.g. via a finite control set MPC [16].

in this section. In order to ensure a time efficient solution, the single subproblems depending on the active constraints are investigated in a combinatorial manner.

A. Problem formulation

The computation of reference currents $\hat{\boldsymbol{i}}_{\mathrm{dq}}$ for a desired torque T_{des} is a non-trivial problem, since the torque expression (2) depends on both dq-currents $(i_{\mathrm{d}}, i_{\mathrm{q}})$ and the nonlinear systems constraints (4)-(6) have to be satisfied.

The principle objective of providing the desired torque – or at least to minimize the deviation in view of the constraints – can be formulated as the optimization problem

$$\mathcal{I} = \arg\min_{i_{\mathrm{d}}, i_{\mathrm{q}}} \quad \left(T_{\mathrm{des}} - T_{\mathrm{D}}(i_{\mathrm{d}}, i_{\mathrm{q}})\right)^2 \tag{7a}$$

$$\text{s.t.} \quad i_{\mathrm{d}}^2 + i_{\mathrm{q}}^2 \leq I_{\mathrm{max}}^2 \tag{7b}$$

$$u_{\mathrm{q}}^2 + u_{\mathrm{q}}^2 \leq U_{\mathrm{max}}^2 \tag{7c}$$

$$\tfrac{3}{2}\tfrac{(i_{\mathrm{d}}u_{\mathrm{d}} + i_{\mathrm{q}}u_{\mathrm{q}})}{U_{\mathrm{dc}}} \leq I_{\mathrm{dc,max}} \tag{7d}$$

$$\tfrac{3}{2}\tfrac{(i_{\mathrm{d}}u_{\mathrm{d}} + i_{\mathrm{q}}u_{\mathrm{q}})}{U_{\mathrm{dc}}} \geq I_{\mathrm{dc,min}}\,. \tag{7e}$$

Note that the minimizing solution of (7) will in general not be an isolated point but a set $\mathcal{I}$. A unique solution $\hat{\boldsymbol{i}}_{\mathrm{dq}}$ over $\mathcal{I}$ is obtained by minimizing the energy losses under the assumption that Joules losses are predominant, i.e.

$$\hat{\boldsymbol{i}}_{\mathrm{dq}} = \arg\min_{\boldsymbol{i}_{\mathrm{dq}} \in \mathcal{I}} \; i_{\mathrm{d}}^2 + i_{\mathrm{q}}^2\,. \tag{8}$$

Note that (7) and (8) form a min-min-problem that differs from the common approach to jointly minimize $(T_{\mathrm{des}} - T_{\mathrm{D}}(i_{\mathrm{d}}, i_{\mathrm{q}}))^2 + r(i_{\mathrm{d}}^2 + i_{\mathrm{q}}^2)$ for some weight $r > 0$. The hierarchical solution of (7) and (8) puts the emphasize on realizing the desired torque T_{des}, while considering energy optimality in a second step.

In order to reduce the complexity of the inner minimization problem (7), the dq-voltages in the constraints (7c)-(7e) are replaced by the stationary system equations (1)

$$u_{\mathrm{d}} = Ri_{\mathrm{d}} - \omega L_{\mathrm{q}} i_{\mathrm{q}} \tag{9a}$$

$$u_{\mathrm{q}} = Ri_{\mathrm{q}} + \omega L_{\mathrm{d}} i_{\mathrm{d}} + \omega\psi_{\mathrm{p}}\,. \tag{9b}$$

Although the optimization problem (7) with (9) is still nonlinear and non-convex, its solution as well as the solution of the overall min-min-problem can be explicitly computed. To solve these problems in an analytical way, the hierarchical optimization is analyzed in the following subsections by considering the unconstrained and constrained cases of (7) separately. The distinction of the single cases leads to the reference current values $\boldsymbol{i}_{\mathrm{dq}}^{\mathrm{A}}, \ldots, \boldsymbol{i}_{\mathrm{dq}}^{\mathrm{F}}$ corresponding to the intersection points A to J in Fig. 2. The following considerations use Fig. 2 to simplify the explanations in the dq-current plane for motor and generator operation, respectively. Section IV then combines the single cases in a combinatorial algorithm to compute the optimal reference $\hat{\boldsymbol{i}}_{\mathrm{dq}}$.

B. Unconstrained case

If no constraints of (7) are active, the desired torque T_{des} is exactly reached and the overall min-min-problem (7), (8)

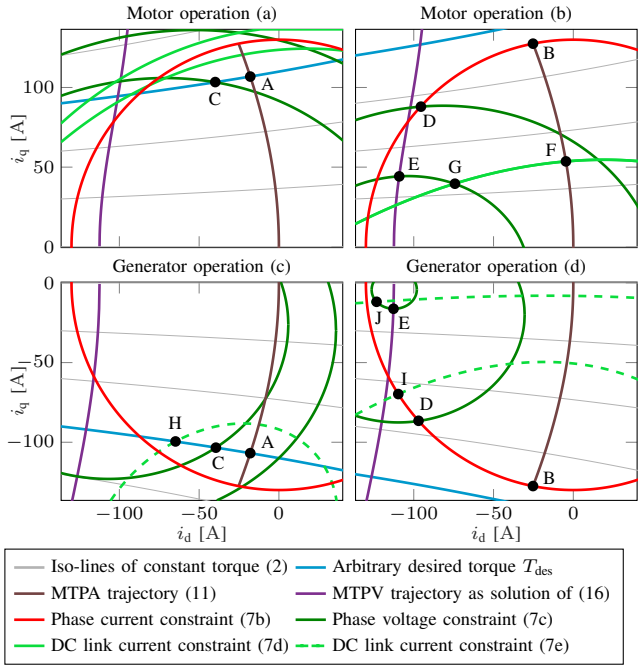

Fig. 2. dq-current plane with boundaries of the constraints for $\omega > 0$ and intersection points A to J using the stationary voltage equations (9).

can be equivalently stated as

$$\min_{i_{\mathrm{d}}, i_{\mathrm{q}}} \quad i_{\mathrm{d}}^2 + i_{\mathrm{q}}^2 \tag{10a}$$

$$\text{s.t.} \quad T_{\mathrm{des}} = \tfrac{3}{2} z_{\mathrm{p}} \left(\psi_{\mathrm{p}} i_{\mathrm{q}} + i_{\mathrm{d}} i_{\mathrm{q}} (L_{\mathrm{d}} - L_{\mathrm{q}})\right). \tag{10b}$$

For any value of T_{des}, the solution lies on the maximum-torque-per-ampere (MTPA) trajectory, implicitly given by

$$i_{\mathrm{d}} + \tfrac{L_{\mathrm{d}} - L_{\mathrm{q}}}{\psi_{\mathrm{p}}}(i_{\mathrm{d}}^2 - i_{\mathrm{q}}^2) = 0\,, \tag{11}$$

see e.g. [4], [11]. Consequently, the optimal operating point $\boldsymbol{i}_{\mathrm{dq}}^{\mathrm{A}}$ is given by the intersection of the MTPA trajectory and the hyperbola corresponding to the desired torque, see point A in Fig. 2 (a) and (c).

C. Active phase current constraint (7b)

The boundary of the phase current constraint (7b)

$$i_{\mathrm{d}}^2 + i_{\mathrm{q}}^2 = I_{\mathrm{max}}^2 \tag{12}$$

is a circle around the origin with radius I_{max}, as shown in Fig. 2. If the desired torque T_{des} is larger than the maximum achievable torque T_{B}, the current constraint becomes active. In this case, the optimal solution $\boldsymbol{i}_{\mathrm{dq}}^{\mathrm{B}}$ minimizing the deviation to T_{des} lies on the intersection point B of the active phase current constraint and the MTPA trajectory (11), which provides the highest torque for a given current $i_{\mathrm{d}}^2 + i_{\mathrm{q}}^2$.Note that the set of equations (11) has four different solutions. Only two of them are meaningful, corresponding to the point B in Fig. 2 (b) and (d).

D. Active phase voltage constraint (7c)

The boundary of the phase voltage constraint (7c) can be expressed as

$$(Ri_{\mathrm{d}} - \omega L_{\mathrm{q}} i_{\mathrm{q}})^2 + (Ri_{\mathrm{q}} + \omega(L_{\mathrm{d}} i_{\mathrm{d}} + \psi_{\mathrm{p}}))^2 = \tfrac{1}{3} U_{\mathrm{dc}}^2 \tag{13}$$

if the stationary voltages (9) are considered. The corresponding curve in the dq-current plane has an ellipsoidal-like shape, cf. Fig. 2, and depends on the rotor speed ω and the DC link voltage. At standstill $\omega = 0$, the boundary of the voltage constraint (13) reduces to the circle

$$R^2(i_\mathrm{d}^2 + i_\mathrm{q}^2) = \tfrac{1}{3}U_\mathrm{dc}^2 \tag{14}$$

that is similar to the phase current constraint (12). With an increasing rotor speed $\omega > 0$ or with a decreasing DC link voltage, the admissible region in the dq-current plane becomes smaller, which can be seen by reformulating (13)

$$\left(\frac{R_\mathrm{s} i_\mathrm{d}}{\omega} - L_\mathrm{q} i_\mathrm{q}\right)^2 + \left(\frac{R_\mathrm{s} i_\mathrm{q}}{\omega} + L_\mathrm{d} i_\mathrm{d} + \psi_\mathrm{p}\right)^2 = \frac{U_\mathrm{dc}^2}{3\,\omega^2}\,. \tag{15}$$

For increasing rotor speeds ω, in particular, the valid region eventually converges to the point $\boldsymbol{i}_\mathrm{dq} = [-\frac{\psi_\mathrm{p}}{L_\mathrm{q}}, 0]^\mathrm{T}$ independent of the DC link voltage.

Two cases have to be distinguished for the computation of the optimal solution. If the curves of the phase voltage constraint (13) and of the desired torque T_des intersect in the dq-plane, cf. point C in Fig. 2 (a) and (c), the optimal solution $\boldsymbol{i}_\mathrm{dq}^\mathrm{C}$ that minimizes the current's magnitude can be determined by solving (2) and (13).

On the other hand, if both curves do not intersect, the desired torque T_des cannot be realized without violating the phase voltage constraint. In this case, the min-min-problem (7), (8) can be written as the optimization problem

$$\min_{i_\mathrm{d}, i_\mathrm{q}} \quad -\operatorname{sign}(T_\mathrm{des})\tfrac{3}{2} z_\mathrm{p}\left(\psi_\mathrm{p} i_\mathrm{q} + i_\mathrm{d} i_\mathrm{q}(L_\mathrm{d} - L_\mathrm{q})\right) \tag{16a}$$

$$\text{s.t.} \quad (R i_\mathrm{d} - \omega L_\mathrm{q} i_\mathrm{q})^2 + (R i_\mathrm{q} + \omega(L_\mathrm{d} i_\mathrm{d} + \psi_\mathrm{p}))^2 = \tfrac{1}{3}U_\mathrm{dc}^2\,, \tag{16b}$$

since there is only one point in the dq-current plane minimizing the deviation to the desired torque. The solution of problem (16) including the reasonable one corresponding to the point $\boldsymbol{i}_\mathrm{dq}^\mathrm{E}$ in Fig. 2 (b) and (d) can be explicitly computed using computer algebra software such as MATHEMATICA.

Note that the solution of (16) lies on the so-called maximum-torque-per-voltage (MTPV) trajectory [17] that is also shown in Fig. 2. Due to the consideration of the stator resistance R, however, no simple function such as in the case of the MTPA trajectory (11) can be given.

E. Active DC link current constraint (7d)

Similar to the voltage constraint, the boundary of the upper DC link current constraint (7d) can be formulated using the stationary voltage equations (9), i.e.

$$\frac{3}{2}\frac{i_\mathrm{d}\left(R i_\mathrm{d} - \omega L_\mathrm{q} i_\mathrm{q}\right) + i_\mathrm{q}\left(R i_\mathrm{q} + \omega L_\mathrm{d} i_\mathrm{d} + \omega\psi_\mathrm{p}\right)}{U_\mathrm{dc}} = I_\mathrm{dc,max}\,, \tag{17}$$

also see Fig. 2 (a) and (b) for an arbitrary rotor speed $\omega > 0$.[3] Note that the intersection of the active upper DC link current constraint (17) with the curve for the desired torque T_des (cf. Fig. 2) cannot occur at an optimal point, as $\boldsymbol{i}_\mathrm{dq}^\mathrm{A}$ corresponding to point A inside this intersection interval of the desired torque curve minimizes (8). Hence, the optimal solution for an active upper DC link current constraint is given by $\boldsymbol{i}_\mathrm{dq}^\mathrm{F}$ as the intersection of (17) and the MTPA trajectory (11).

[3]The upper DC link current constraint is not relevant in generator operation (Fig. 2 (c) and (d)) from a practical point of view, as it would imply that power loss in the motor is larger than its brake power.

F. Active DC link current constraint (7e)

The lower bound of the DC link current constraint

$$\frac{3}{2}\frac{i_\mathrm{d}\left(R i_\mathrm{d} - \omega L_\mathrm{q} i_\mathrm{q}\right) + i_\mathrm{q}\left(R i_\mathrm{q} + \omega L_\mathrm{d} i_\mathrm{d} + \omega\psi_\mathrm{p}\right)}{U_\mathrm{dc}} = I_\mathrm{dc,min} \tag{18}$$

can be stated similarly to (17). In this case, however, the admissible and inadmissable sets of the constraint are interchanged and the lower bound $I_\mathrm{dc,min}$ is usually less or equal to zero. Consequently, in motor operation, where $\omega\, T_\mathrm{des} \geq 0$ by definition, the constraint cannot become active, as a reformation of (18)

$$\frac{3}{2}\frac{R\left(i_\mathrm{d}^2 + i_\mathrm{q}^2\right) + \omega\left(i_\mathrm{q}\left(\psi_\mathrm{p} + i_\mathrm{d}(L_\mathrm{d} - L_\mathrm{q})\right)\right)}{U_\mathrm{dc}} = I_\mathrm{dc,min} \tag{19}$$

shows. Moreover, at zero or low speeds the stationary inequality

$$\frac{3}{2}\frac{R(i_\mathrm{d}^2 + i_\mathrm{q}^2)}{U_\mathrm{dc}} \geq I_\mathrm{dc,min} \tag{20}$$

holds for all currents. For increasing rotor speeds ω, however, the inadmissable set grows and the boundary eventually converges to the straight line $i_\mathrm{q} = 0$, as indicated in Fig. 2 (c) and (d).

Looking at the reference value computation, this means that every desired torque T_des can be realized for all (finite) rotor speeds ω. If the lower DC link current constraint is active, there are two intersection points of the constraint boundary and the desired torque hyperbola, see Fig. 2 (c) and (d). The two points are possible solutions of the min-min-problem (7), (8) and can be computed by solving the equations (2) and (19). In general, both points are equally efficient in terms of (8). This can be seen by reformulating (19)

$$\frac{3}{2}\frac{R(i_\mathrm{d}^2 + i_\mathrm{q}^2)}{U_\mathrm{dc}} + \frac{\omega T_\mathrm{des}}{z_\mathrm{p} U_\mathrm{dc}} = I_\mathrm{dc,min}\,, \tag{21}$$

which shows that $i_\mathrm{d}^2 + i_\mathrm{q}^2$ are identical for both intersection points. In view of the phase voltage constraint, which enforces d-currents less than zero, it is reasonable to choose the intersection with the smaller d-current value, i.e. $\boldsymbol{i}_\mathrm{dq}^\mathrm{H}$ corresponding to point H in Fig. 2 (c). This ensures continuity of the reference values for the dq-currents in continuous-time of the PMSM operation.

G. Case of multiple active constraints

In case of two active constraints, the solution of the optimization problem (7) is in general unique, which also renders the superior minimization problem (8) trivial. Depending on which constraints are active, the optimal solution is obtained by solving the corresponding set of equations and choosing the reasonable solution. Table I shows the possible combination of active constraints, the set of equations to be solved, and the corresponding points illustrated in Fig. 2 (b) and (d). Note that more than two constraints can become

TABLE I

POSSIBLE COMBINATION OF TWO ACTIVE CONSTRAINTS.

active constraints	set of equations	point in Fig. 2
(7b) & (7c)	(12) & (13)	D
(7c) & (7d)	(13) & (17)	G
(7c) & (7e)	(13) & (18)	J
(7b) & (7e)	(12) & (18)	I

active at the same time, i.e. (7b)-(7d) or (7b), (7c), (7e), respectively. However, two active constraints are sufficient to determine the optimal point.

From a theoretical point of view, the min-min-problem (7), (8) can be unsolvable, if the point $\boldsymbol{i}_{\mathrm{dq}} = [-\frac{\psi_{\mathrm{p}}}{L_{\mathrm{q}}}, 0]^{\mathrm{T}}$, to which the voltage constraint converges for high rotor speeds, see (15), does not satisfy the constraints (7b) and (7d).[4] In this case, a rotor speed ω_{max} exists, where the admissible set of dq-currents becomes empty. From a practical point of view, however, rotor speeds above ω_{max} are typically prevented constructively and are therefore not considered in the following.

IV. SOLUTION DETERMINATION

The previous section successively discussed the possible solutions of the optimization problems (7) and (8). This section presents an algorithm to determinate which of the possible solutions is the correct one. Although the algorithm is presented for machines with reluctance torque, it can easily be applied to reluctance-free machines with some slight modification concerning the handling of the upper DC link current constraint.

A. Basic algorithm

Fig. 3 shows a flow chart of the proposed algorithm that is detailed in this section. The solution is primarily determined on the basis of the d-currents i_{d}, in order to minimize the computational effort.

At the beginning, the maximum torque T_{B} corresponding to the point $\boldsymbol{i}_{\mathrm{dq}}^{\mathrm{B}}$ is computed and the desired torque is limited to the set $[-T_{\mathrm{B}}, T_{\mathrm{B}}]$, since higher or lower torque demands cannot be realized.

The next step of the algorithm checks whether the machine is in motor or generator operation and the d-currents of the relevant points, i.e. ($i_{\mathrm{d}}^{\mathrm{A}}$, $i_{\mathrm{d}}^{\mathrm{C}}$, $i_{\mathrm{d}}^{\mathrm{D}}$, $i_{\mathrm{d}}^{\mathrm{E}}$) and depending on the operating mode either ($i_{\mathrm{d}}^{\mathrm{F}}$, $i_{\mathrm{d}}^{\mathrm{G}}$) or ($i_{\mathrm{d}}^{\mathrm{H}}$, $i_{\mathrm{d}}^{\mathrm{I}}$, $i_{\mathrm{d}}^{\mathrm{J}}$) are evaluated. In the case that one of the intersection points does not exist for the given parameter set, the corresponding d-current is set to NaN and is therefore ignored in the further considerations.

The next two subsections describe the distinct branches of the algorithm in Fig.3 for motor and generator operation mode, respectively.

B. Motor operating mode

In motor operation, i.e. $\omega T_{\mathrm{des}} \geq 0$, the point $\boldsymbol{i}_{\mathrm{dq}}^{\mathrm{F}}$ is further investigated. Since $\boldsymbol{i}_{\mathrm{dq}}^{\mathrm{F}}$ only depends on the maximum DC link current $I_{\mathrm{dc,max}}$, it is necessary to compute $i_{\mathrm{q}}^{\mathrm{F}}$ and evaluate whether it violates the voltage constraint (13). In this case, the point $\boldsymbol{i}_{\mathrm{dq}}^{\mathrm{F}}$ can be neglected and $i_{\mathrm{d}}^{\mathrm{F}}$ is set to NaN.

[4]Note that the constraint (7d) is independent of ω if $i_{\mathrm{q}} = 0$.

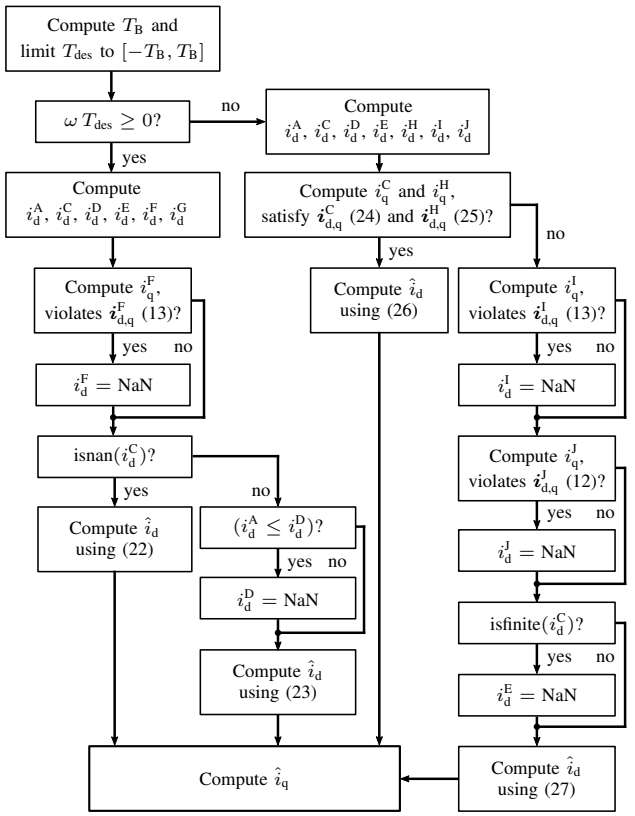

Fig. 3. Flow chart of the reference value computation algorithm.

The next step of the algorithm consists in checking the point $\boldsymbol{i}_{\mathrm{dq}}^{\mathrm{C}}$. If $i_{\mathrm{d}}^{\mathrm{C}}$ is NaN, the desired torque T_{des} cannot be reached and only the points $\boldsymbol{i}_{\mathrm{dq}}^{\mathrm{D}}$, $\boldsymbol{i}_{\mathrm{dq}}^{\mathrm{E}}$, $\boldsymbol{i}_{\mathrm{dq}}^{\mathrm{F}}$, and $\boldsymbol{i}_{\mathrm{dq}}^{\mathrm{G}}$ remain relevant for finding the optimal solution. In that case, the correct solution of the d-current is given by

$$\hat{i}_{\mathrm{d}} = \max\left\{i_{\mathrm{d}}^{\mathrm{D}}, i_{\mathrm{d}}^{\mathrm{E}}, \min\left\{i_{\mathrm{d}}^{\mathrm{F}}, i_{\mathrm{d}}^{\mathrm{G}}\right\}\right\} . \tag{22}$$

The maximization guarantees that the optimal solution $\hat{i}_{\mathrm{d}}$ provides the maximum possible torque, as it can be seen in Fig. 2 (b). The compliance with the phase current constraint is ensured, since the d-current of all points $\boldsymbol{i}_{\mathrm{dq}}^{\mathrm{E}}$ violating the phase current constraint is smaller than $i_{\mathrm{d}}^{\mathrm{D}}$. Moreover, the optimal solution $\hat{i}_{\mathrm{d}}$ complies with the voltage constraint and satisfies the DC link current constraint (7d) as well, because the d-currents of all points $\boldsymbol{i}_{\mathrm{dq}}^{\mathrm{G}}$ and $\boldsymbol{i}_{\mathrm{dq}}^{\mathrm{E}}$ violating this constraint are smaller than $i_{\mathrm{d}}^{\mathrm{G}}$ or $i_{\mathrm{d}}^{\mathrm{F}}$.

If $i_{\mathrm{d}}^{\mathrm{C}}$ is not NaN but a finite value, the points $\boldsymbol{i}_{\mathrm{dq}}^{\mathrm{A}}$, $\boldsymbol{i}_{\mathrm{dq}}^{\mathrm{D}}$, $\boldsymbol{i}_{\mathrm{dq}}^{\mathrm{F}}$ and $\boldsymbol{i}_{\mathrm{dq}}^{\mathrm{G}}$ must be considered. If $i_{\mathrm{d}}^{\mathrm{D}} > i_{\mathrm{d}}^{\mathrm{A}}$, the point $\boldsymbol{i}_{\mathrm{dq}}^{\mathrm{D}}$ is irrelevant and set to NaN. The correct solution under this precondition is

$$\hat{i}_{\mathrm{d}} = \max\left\{\min\left\{i_{\mathrm{d}}^{\mathrm{A}}, i_{\mathrm{d}}^{\mathrm{C}}\right\}, i_{\mathrm{d}}^{\mathrm{D}}, \min\left\{i_{\mathrm{d}}^{\mathrm{F}}, i_{\mathrm{d}}^{\mathrm{G}}\right\}\right\} . \tag{23}$$

The solution satisfies all constraints using similar arguments as discussed in the previous case.

C. Generator operating mode

In generator operation, i.e. $\omega T_{\text{des}} < 0$, the algorithm follows the right branch in Fig. 3 and again starts with a case discrimination, whether the desired torque T_{des} is realizable or not. This is done by computing the q-currents of the points $\boldsymbol{i}_{\text{dq}}^{\text{C}}$ and $\boldsymbol{i}_{\text{dq}}^{\text{H}}$. In view of the constraints (7b)-(7e), the desired torque T_{des} is realizable under the following conditions: the point $\boldsymbol{i}_{\text{dq}}^{\text{C}}$ exists, the condition

$$\left(\left(i_{\text{d}}^{\text{C}}\right)^2 + \left(i_{\text{d}}^{\text{C}}\right)^2 \leq I_{\text{max}}^2\right) \vee \left(i_{\text{d}}^{\text{C}} > i_{\text{d}}^{\text{A}}\right) \tag{24}$$

holds, and either the point $\boldsymbol{i}_{\text{dq}}^{\text{H}}$ does not exist (i_{d}^{H} is NaN) or the condition

$$\left(\left(i_{\text{d}}^{\text{H}}\right)^2 + \left(i_{\text{d}}^{\text{H}}\right)^2 \leq I_{\text{max}}^2\right) \wedge \Bigg(i_{\text{d}}^{\text{C}} < i_{\text{d}}^{\text{H}} \vee \left(\left(Ri_{\text{d}}^{\text{H}} - \omega L_{\text{q}} i_{\text{q}}^{\text{H}}\right)^2 + \left(Ri_{\text{q}}^{\text{H}} + \omega\left(L_{\text{d}} i_{\text{d}}^{\text{H}} + \psi_{\text{p}}\right)\right)^2 \leq U_{\text{max}}^2\right)\Bigg) \tag{25}$$

holds. The first condition (24) requires point $\boldsymbol{i}_{\text{dq}}^{\text{C}}$ to lie within the admissible set of the phase current constraint or "to the right" of the MTPA trajectory, cf. Fig. 2 (a) or (c). The second one (25) requires the point $\boldsymbol{i}_{\text{dq}}^{\text{H}}$ to satisfy the phase current constraint (7b) and either to comply with the voltage constraint (7c) or to be on the right side of point $\boldsymbol{i}_{\text{dq}}^{\text{C}}$.

If T_{des} is realizable, the optimal solution

$$\hat{i}_{\text{d}} = \min\left\{i_{\text{d}}^{\text{A}}, i_{\text{d}}^{\text{C}}, i_{\text{d}}^{\text{H}}\right\} \tag{26}$$

follows intuitively. If T_{des} is not realizable, it has to be ensured that the points $\boldsymbol{i}_{\text{dq}}^{\text{I}}$ and $\boldsymbol{i}_{\text{dq}}^{\text{J}}$ satisfy the phase voltage and current constraints (7c) and (7b), respectively. The corresponding d-current is set to NaN, if this condition is violated. Moreover, i_{d}^{E} is set to NaN if i_{d}^{C} exists, since in this case the point i_{d}^{E} cannot be the solution, even if $\boldsymbol{i}_{\text{dq}}^{\text{C}}$ violates the phase current constraint. With these preliminary considerations, the optimal solution eventually follows to

$$\hat{i}_{\text{d}} = \min\left\{\max\left\{i_{\text{d}}^{\text{D}}, i_{\text{d}}^{\text{E}}\right\}, \max\left\{i_{\text{d}}^{\text{I}}, i_{\text{d}}^{\text{J}}\right\}\right\} \tag{27}$$

and satisfies all constraints, as Fig. 2 (d) illustrates.

V. Evaluation

The performance of the algorithm for computing the reference currents is evaluated in terms of computational speed and using simulation studies. In particular, an efficient numerical execution of the algorithm is important to allow for a future embedded real-time implementation on industrial PMSM control hardware.

A. Computation time analysis

The algorithm is implemented under C. The explicit solutions for the single points $\boldsymbol{i}_{\text{dq}}^{k}$, $k \in \{\text{A}, \ldots, \text{J}\}$ are computed using the computer algebra software MATHEMATICA and are exported as optimized C code.

Since the computation time of the algorithm is crucial, especially on the hardware that is typically used in electric machine control, several investigation were performed. Table II shows the computation time of the proposed algorithm on a standard laptop CPU (Intel i7-5600U @ 2.60 GHz) and on the dSPACE real-time system DS 1202. The analysis was performed for single and double floating point precision as well as for machines with and without reluctance torque, i.e. $L_{\text{d}} \neq L_{\text{q}}$ or $L_{\text{d}} = L_{\text{q}}$.

The computation times for machines without reluctance torque are about four times smaller. The reason is that the expressions for computing the different current points $\boldsymbol{i}_{\text{dq}}^{k}$, $k \in \{\text{A}, \ldots, \text{J}\}$ are significantly more complex in case of different values for the inductivities. Moreover, the conditioning of the numerical computations for machines with reluctance torque is very sensitive and therefore requires double precision algorithmics to obtain accurate results. In view of an embedded implementation, this gives further optimization potential, since the computation for machines without reluctance torque at single precision is more than 15 % faster compared to double precision.

In summary, the computation time in all considered cases is below 10 µs, which shows the algorithmic efficiency of the reference computation and therefore proves the suitability of the algorithm for embedded implementations.

TABLE II
COMPUTATION TIME ANALYSIS WITH SINGLE (S) AND DOUBLE (D) PRECISION, DIFFERENT MOTOR TYPES, AND OPERATING MODES.

	motor operation		generator operation	
	$L_{\text{d}} \neq L_{\text{q}}$	$L_{\text{d}} = L_{\text{q}}$	$L_{\text{d}} \neq L_{\text{q}}$	$L_{\text{d}} = L_{\text{q}}$
PC (d)	1.3 µs	0.3 µs	1.6 µs	0.3 µs
dSpace (s)	-	1.6 µs	-	1.9 µs
dSpace (d)	7.8 µs	1.9 µs	9.2 µs	2.2 µs

B. Simulation results

The algorithm was tested for given time profiles of the rotor speed ω and desired torque T_{des} based on measurements from an actual PMSM with a field oriented controller. Figure 4 shows the trajectories of ω and T_{des} along with the reference currents $\hat{\boldsymbol{i}}_{\text{dq}} = [\hat{i}_{\text{d}}, \hat{i}_{\text{q}}]^{\mathsf{T}}$ and voltages $\hat{\boldsymbol{u}}_{\text{dq}} = [\hat{u}_{\text{d}}, \hat{u}_{\text{q}}]^{\mathsf{T}}$ as well as the corresponding driving torque T_{D} and DC link current I_{dc}. In addition, Fig. 4 shows the maximum realizable torque T_{max} for each time step that is obtained by numerically solving the optimization problem (7) for an arbitrarily high value of T_{des}. The right side of Fig. 4 illustrates the computed reference currents $\hat{\boldsymbol{i}}_{\text{dq}}$ in the dq-current plane.

In the first milliseconds of the simulation, the MTPA trajectory is exactly tracked, see Fig. 4, until the voltage constraint and afterwards the phase current constraint become active. Two milliseconds later, the lower DC link current constraint becomes active and the magnitude of the dq-voltages is lowered, as it can be seen in Fig. 4. After about $t = 50$ ms, the phase current constraint becomes inactive and the desired torque T_{des} is realized in an energy efficient manner while still keeping the lower DC link current constraint active. After $t = 65$ ms, the voltages constraint becomes active instead of the DC link current constraint.

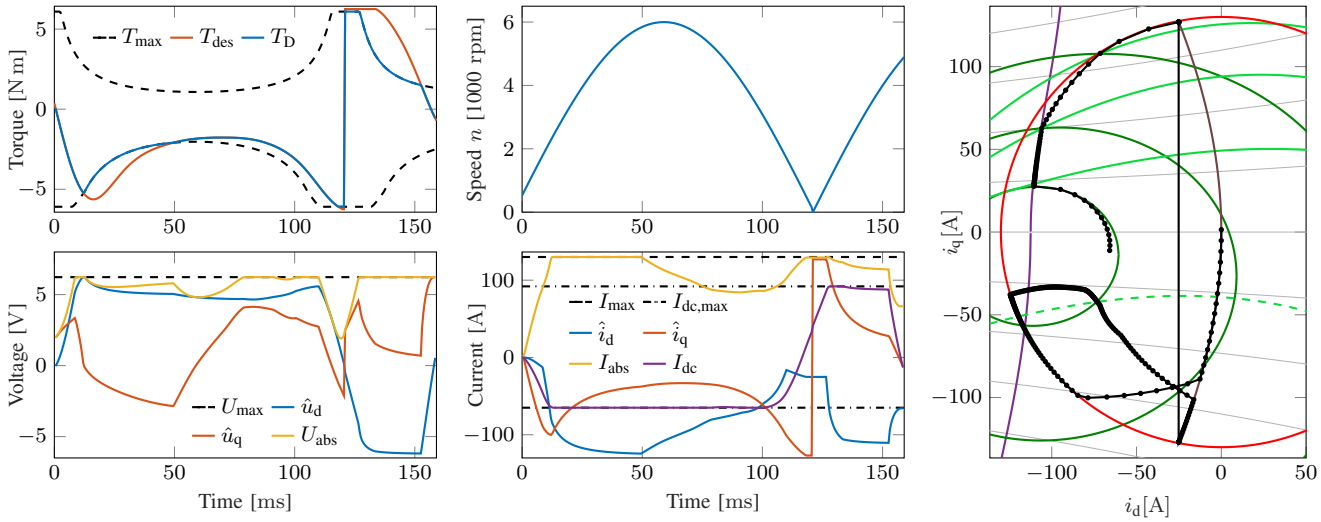

Fig. 4. Simulation results of the current reference value computation as time profiles (left) and in the dq-current plane (right). The color formatting in the dq-current plane corresponds to Fig. 2.

The MTPA trajectory is eventually reached again, as the rotor speed ω decreases.

At $t \approx 120$ms, the desired torque turns positive. Fig. 4 shows that at first the phase current constraint and afterwards the voltage constraint become active while the rotor speed ω increases. After a few milliseconds, a speed of $1050\,\mathrm{rpm}$ is reached and the upper DC link current constraint becomes active instead of the phase current constraint. At the approximate rotor speed $\omega \approx 1850\,\mathrm{rpm}$, the DC link current is lowered and the MTPV trajectory is tracked, until the desired torque T_{des} is realizable again after about $155\,\mathrm{ms}$ at rotor speed $\omega \approx 4350\,\mathrm{rpm}$.

In summary, the simulation results show that the references satisfy all constraints and either the desired or the maximum or minimum realizable torque is provided in an energy optimal manner.

VI. Conclusions

A novel reference current computation scheme for PMSMs is presented that is based on the formulation of a hierarchical nonlinear optimization problem. In contrast to existing approaches, the proposed scheme covers the whole operating range of the machines while ensuring compliance with constraints on the phase currents and voltages as well as on the DC link current. The algorithm has a minimal computational complexity thanks to the analytic combinatorial solution of the min-min-problem. Simulation and computation time results show the performance and the suitability of the algorithm for an embedded implementation

Further work concerns an improvement of the numerics in order the solve the optimization problem for all PMSM motor types using single precision as well as a seamless integration of the algorithm for the reference current computation within a real-time nonlinear model predictive control scheme.

Acknowledgment

The authors gratefully thank the Robert Bosch Automotive Steering GmbH for the support.

References

[1] N. P. Quang and J.-A. Dittrich, *Vector Control of Three-Phase AC Machines*. Berlin, Germany: Springer, 2008.

[2] N. Hamano and H. Nakamura, "Global dynamic maximum torque per ampere control of interior permanent magnet synchronous motor by using nonsmooth control Lyapunov function," in *Proc. 20th IFAC World Congress*, Toulouse, France, 2017, pp. 2405–8963.

[3] D. Faustner, W. Kemmetmüller, and A. Kugi, "Flatness-Based Torque Control of Saturated Surface-Mounted Permanent Magnet Synchronous Machines," *IEEE Trans. Contr. Syst. Techn.*, no. 99, pp. 1–13, 2015.

[4] M. Preindl and S. Bolognani, "Model Predictive Direct Torque Control With Finite Control Set for PMSM Drive Systems, Part 1: Maximum Torque Per Ampere Operation," *IEEE Trans. Ind. Informat.*, vol. 9, no. 4, pp. 1912–1921, 2013.

[5] S. Chai, L. Wang, and E. Rogers, "Model Predictive Control of a Permanent Magnet Synchronous Motor With Experimental Validation," *Contr. Eng. Pract.*, vol. 21, no. 11, pp. 1584–1593, 2013.

[6] J. Rodriguez, M. P. Kazmierkowski, J. R. Espinoza, P. Zanchetta, H. Abu-Rub, H. A. Young, and C. A. Rojas, "State of the Art of Finite Control Set Model Predictive Control in Power Electronics," *IEEE Trans. Ind. Informat.*, vol. 9, no. 2, pp. 1003–1016, 2013.

[7] T. Geyer and D. E. Quevedo, "Multistep Finite Control Set Model Predictive Control for Power Electronics," *IEEE Trans. Power Electron.*, vol. 29, no. 12, pp. 6836–6846, 2014.

[8] T. Englert, S. Grüner, and K. Graichen, "Model predictive torque control of permanent magnet synchronous machines," in *Proc. 20th IFAC World Congress*, Toulouse, France, 2017, pp. 758–763.

[9] J. Köhler, M. Manderla, and F. Malchow, "Embedded model predictive direct switching control for high performance electrical drives - a quantitative comparison," in *Proc. 20th IFAC World Congress*, Toulouse, France, 2017, pp. 11 871–11 876.

[10] S. Bolognani, S. Calligaro, and R. Petrella, "Adaptive Flux-Weakening Controller for Interior Permanent Magnet Synchronous Motor Drives," *IEEE Trans. Emerg. Sel. Topics Power Electron.*, vol. 2, no. 2, pp. 236–248, 2014.

[11] D. Schröder, *Regelung von Antriebssystemen*, 3rd ed. Berlin, Germany: Springer, 2009.

[12] M. Preindl and S. Bolognani, "Optimal State Reference Computation With Constrained MTPA Criterion for PM Motor Drives," *IEEE Trans. Power Electron.*, vol. 30, no. 8, pp. 4524–4535, 2015.

[13] S. L. Kellner and B. Piepenbreier, "General PMSM d,q-model using optimized interpolated absolute and differential inductance surfaces," in *IEEE Int. Electr. Mach. Drives Conf.*, Niagara Falls, Canada, 2011, pp. 212–217.

[14] S. Ebersberger and B. Piepenbreier, "Identification of differential inductances of permanent magnet synchronous machines using test current signal injection," in *Int. Symp. Power Electron., Electr. Drives, Auto. and Motion*, Sorrento, Italy, 2012, pp. 1342–1347.

[15] F. Qi, A. Stippich, S. Koschik, and R. W. D. Doncker, "Model predictive overload control of induction motors," in *IEEE Int. Conf. Electr. Mach. Drives*, Coeur d'Alene, USA, 2015, pp. 999–1005.

[16] T. Geyer and D. E. Quevedo, "Performance of Multistep Finite Control Set Model Predictive Control for Power Electronics," *IEEE Trans. Power Electron.*, vol. 30, no. 3, pp. 1633–1644, 2015.

[17] M. Preindl and S. Bolognani, "Model Predictive Direct Torque Control With Finite Control Set for PMSM Drive Systems, Part 2: Field Weakening Operation," *IEEE Trans. Ind. Electron.*, vol. 9, no. 2, pp. 648–657, 2013.